Full-field and point strain measurement via the inner surface of a rolling large lug tyre

Megan S. Pegram, Theunis R. Botha and P. Schalk Els

Vehicle safety and performance can be dramatically improved if force or friction measurement of the tyre-terrain interface is known. Since the tyre-terrain interface is responsible for the majority of forces acting on the vehicle, this region has received a lot of attention in vehicle dynamics. Direct measurement of the tyre-terrain interface is difficult since it is hidden by the tyre and terrain. A lot of research has been conducted on the inside of tyre using accelerometers or strain gauges with research more focussed on passenger car tyres and very little work performed on agricultural tyres with larger lugs. This study performs strain measurements using point measurement, from strain gauges, and full field measurement, using a stereo camera measurement system, of the inside of an agricultural tyre on a drum test rig during vertical and lateral loading. Results show similar trends when compared to results on passenger car tyres, however the mounting of the strain gauge relative to the lug is shown to play a large role in the developed strain. Linear relationships between the applied tyre force and strain were obtained in different direction with R^2 values above 0.97.

1. Introduction

Current active safety systems extract very little direct information from the tyre, which is where most forces enter the vehicle. Extending measurements to estimate tyre contact forces and other parameters, such as slip angle, longitudinal slip and friction coefficient can greatly improve vehicle control. Tyre measurement hubs have been used to measure contact forces through the wheel hub (Hamersma et al, 2016), commonly called Wheel Force Transducers (WFT). While the measurement hubs are capable of measuring all forces produced by the tyre. The hubs are, however, expensive and add additional inertia, which limits their commercial use. Vehicle dynamic research have thus focussed on estimating vehicle forces and parameters rather than directly measuring the forces (Acosta et al, 2017). Such estimations are typically only reliable during extreme manoeuvres, which induces large sensor excitations. Friction coefficient estimation methods perform best when the full friction potential of the tyre is used

and thus often perform poorly on low friction surfaces (Khaleghian et al, 2017). Estimating tyre forces directly from the tyre-road interface will undoubtedly provide benefits over estimation techniques. These benefits may include extending reliable measurement capabilities to low speed and low friction surfaces, as well as, producing more direct measurements thus reducing the number of assumption required in estimation techniques. Measuring the outside tyre surface is however, a complex task as it is obscured by the terrain and may operate in changing environmental conditions. Thus, many measurement techniques take measurement of the inner surface of the tyre due to it being a sealed and protected environment and not being obscured by the terrain. The inner surface is only removed from the outside surface by the tread, which on passenger car tyres is relatively thin. However, agricultural tyres have a much thicker tread and this assumption may not be as valid. Measurements performed on the inner surface of the tyre commonly include acceleration, deflection or strain. These measurements are then used to estimate tyre properties or states.

Tri-axial accelerometers have been selected in numerous studies as they are relatively simple and expensive sensors (Braghin et al., 2006, Niskanen and Tuononen, 2014, Matilainen and Tuononen, 2015). Accelerometers are favourable due to their robustness, small size, cost, insensitivity to temperature and low power requirement. In the studies, acceleration measurements showed sensitivity to vertical load, inflation pressure, camber, slip angle, speed and road roughness. The vehicle speed and road roughness were seen to have a significant effect on the noise level of the acceleration measurements. Since acceleration measurements are also coupled with rotational, vibrational and gravitational accelerations and therefore require advanced post-processing techniques to extract useful data of the tyre-terrain interaction.

Pohl et al. (1999) showed surface acoustic wave (SAW) sensors can be used to measure the tyre deflection and was shown to have potential in measuring surface friction. Piezoelectric sensors (Lee et al., 2015) have also shown promise in determining tyre inflation pressure from deflection measurements. Matsuzaki et al. (2005) showed that by utilising the existing tyres steel reinforcing wires as capacitive sensing elements measurements of the tread deformation could be made. However, some agricultural tyre use nylon reinforcement cords rather than steel making the method in-plausible on such tyres.

Since rubber is significantly less stiff than steel it undergoes large deformation. Thus, many of the studies developed or used sensors specific for a rubber application which would experience large deformations. Matching properties aid in prolonged sensor life as well as more reliable measurements. Commercially bought strain gauges have been used in several studies to measured the strain on the inside of the tyre (Garcia-Pozuelo et al., 2017a, Garcia-Pozuelo et al., 2019 and Morinaga et al., 2006). Custom flexible capacitive strain sensors with properties made suitable for an in-tyre application were used by Matsuzaki and Todoroki (2007) and Cao et al. (2016). Strain gauges are favourable due to their low cost and high sampling rate. Strain gauges can also be wired in numerous configurations in order to eliminate or include certain measurements (e.g. temperature or bending moments). However, many configurations are not plausible within a tyre due to loading conditions and non-uniform strain. Thus, many studies use strain gauge configurations without temperature compensation and remove temperature affects by other means. Special ranges of strain gauges allow for large elongations, which is important to ensure the strain gauges can deform with the measured surface and does not debond from the surface. Strain gauge measurement noise level is much lower than that of accelerometers (Garcia-Pozuelo et al., 2019) and were shown not to be as sensitive to rotational speed as accelerometers. Variation in speed, inflation pressure, vertical load, camber angle, slip angle and slip ratio were all seen to show effects on strain measurement.

Non-contact full-field measurement of the strain distribution of the inner tyre surface have also been performed using non contact optical techniques. Hiraoka et al. (2009) proposed measuring out-of-plane deformation and in-plane strain with a single camera and a laser to create a speckle pattern. The method required two successive images, with and without the laser, in order to remove the effects of radial displacement caused by out-of-plane motion. This, however, is not possible on a normally rotating tyre. Green (2011) attempted to rectify this, however, could only improve the accuracy with a finer sub-pixel interpolation algorithm. The trends seen by Green (2011) showed a noticeable increase in strain with an increase in vertical displacement of the inner tyre surface.

All the above strain-based tyre studies have been performed on passenger car tyres which have a uniform tread pattern. Armstrong et al. (2015) performed strain measurements on relatively smooth and large lugged robotic tyres and concluded that the lugs may affect the strain measurements. Strain measurements have focussed on the measurement of individual points on passenger tyres. While valuable information is obtained, full field measurement

have the potential to provide a clearer picture of the whole contact patch which is vital in large lugged tyres as shown by Feldesi et al. (2020). Feldesi et al. (2020) performed strain measurements on the inner surface of a static large lugged agricultural tyre, using two cameras inside of the tyre. In the interest of developing a tyre, which can be used to estimate forces, it is important to develop the relationship between strain measurement and tyre, loading conditions. It is also ideal if the relationships are linear in nature. Feldesi et al. (2020) observed that the lug pattern of the tyre has a significant effect on the strain fields produced with large strain concentration found near lugs. The study was however still able to obtain linear relationships between point strain measurements and the applied loads during static tests. The study was however not able to determine whether the pattern of the tyre lugs in contact with the terrain also affects measurements.

All the studies above showed promising trends in the measurements which can be used in the development of a tyre which can estimate important tyre parameters and states. Most strain measurements have focussed on the measurement of specific points on passenger tyres. While point measurements provide valuable, full-field measurement has the potential to provide a clearer picture of the whole contact patch, which is vital in large lugged tyres as shown by Feldesi et al. (2020). Strain gauges showed great promise in measuring changes in tyre states, this however requires additional post-processing of the signals to extract the relevant features. Stereo camera systems can measure full-field strain, equivalent to a multitude of strain gauges, in a non-contact means. However, the post-processing of camera images is significant and limits real-time implementation. The method however shows potential in giving a larger overall picture of the inner surface strain which is useful for research purposes. The main contributions of this paper is single and full-field strain measurements of an agricultural tyre on a dynamic drum test rig during vertical loading and at different slip angles. Relationships of key features in the strain profile are obtained to determine the suitability of strain measurements to determine different tyre states. The effect the lug pattern in contact with the terrain has on the observed strain pattern is also studied.

2. Material and Methods

2.1 Full-field strain measurement system (T2Cam)

A strain-based tyre measurement system, developed by the Vehicle Dynamics Group at the University of Pretoria, provides an in-tyre measurement system of the inner tyre surface. The system, initially developed by Guthrie et al. (2017), comprises of two stereo cameras and an on-board computer mounted on a stabilisation mechanism within the tyre. The data acquisition system makes use of two high speed PointGrey Flea3 (FL3-U3-13Y3M-C) cameras with Kowa LMN4NCL wide angle lenses to capture the entire region in contact with the terrain. The system is called the Tyre-Terrain Camera system or T2Cam. The mechanical stabilisation allows the position of the cameras to remain facing the region in contact with the test surface irrespective of the wheel rotational angle. A schematic of the installed system is given in Figure 1(a). A later iteration of the system, shown in Figure 1(b), positions one camera facing the leading and trailing edge of the contact patch and includes additional lighting, as implemented by Feldesi et al. (2020).

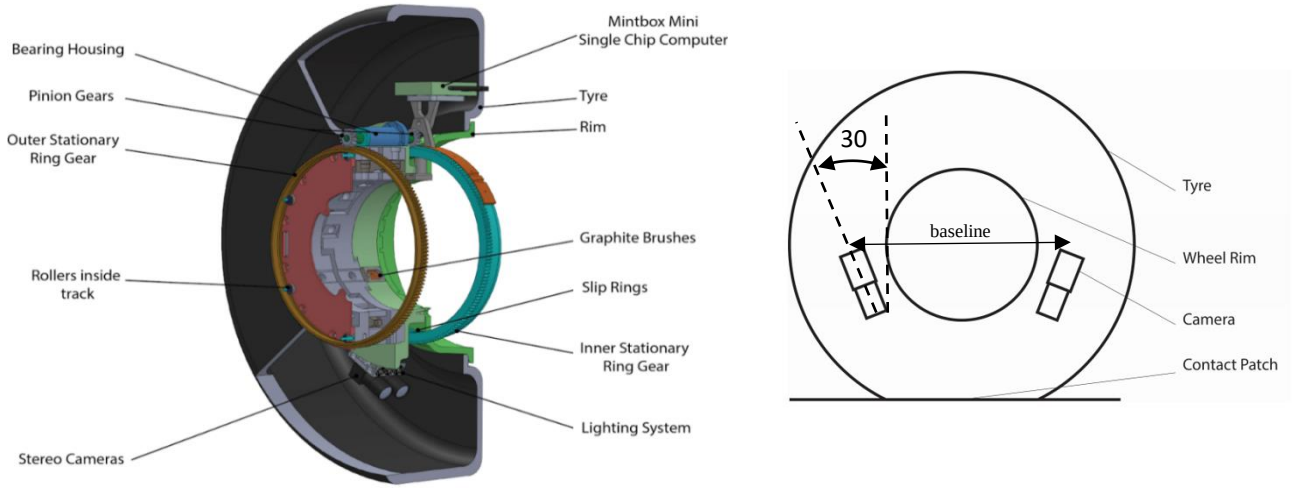

(a) (b)

Figure 1: (a) Schematic of Tyre-terrain camera (T2Cam) with side by side cameras, (b) later iteration of T2Cam with wider baseline between cameras

An inner and outer pair of a planetary and sun gears are used to keep the camera system stationary, allowing the wheel to rotate while the cameras remain in the same position. Detail of the stabilisation system can be found in

Feldesi et al. (2020) . A trigger mechanism is used to take images as the wheel rotates. The trigger consists of a 172-teeth ring machined on the inside of the rim with an infra-red displacement sensor mounted on the stationary sun gear. As the wheel rotates the infra-red sensor moves across the toothed ring which produces a pulse over every tooth on the ring. This results in an image captured approximately every 2° from the two cameras. The two cameras are synchronized to capture at the same time using the same trigger. Lighting is provided by 200W LED lights around each camera lens. The LEDs are strobed, using the trigger pulse, in order to reduce motion blur and power usage.

2.2 Deformation and Strain algorithm

Images from the two camera pair (left and right camera) are passed to a Digital Image Correlation (DIC) algorithm which makes use of the inverse computation Gauss-Newton digital image correlation algorithm (Botha et al. 2017, Baker and Matthews, 2004). This produces a three-dimensional (3D) point cloud of the inner tyre surface from a two-dimensional (2D) image pair. An example of such a point cloud is shown in Figure 2, which shows the inner surface of a tyre while inflated and unloaded. The size of the measured region encompasses the entire region in contact with the terrain. The deformation between two states are determined from the two image pairs provided, the first is a reference state which is taken as un-deformed and the second is a deformed state. It should be noted that the reference state could be any state and it need not be a fully undeformed state. The deformation is simply measured relative to the reference state and shows the additional deformation experienced between the two states, more detail of the algorithm can be found in Guthrie et al. (2016) and Feldesi et al. (2020). In this study the reference state is taken as an inflated tyre with no external loads applied. Constant strain triangles are used to determine in-plane strain from the deformation measurements (Feldesi et al. 2020).

Figure 2: Produced 3D Contact patch: Side view (left), Top view (middle), Isometric view (right)

2.3 Strain gauge placement

Strain gauges can measure tension and compression using the elongation and contraction of the applied surface by measuring the change in resistance across the gauge. Point strain measurements have been performed in several free rolling passenger car tyre studies and have shown similar trends in these studies. Morinaga et al. (2006) illustrates the typical strain distribution of a point measurement as experienced for a full revolution in a passenger car tyre in Figure 3.

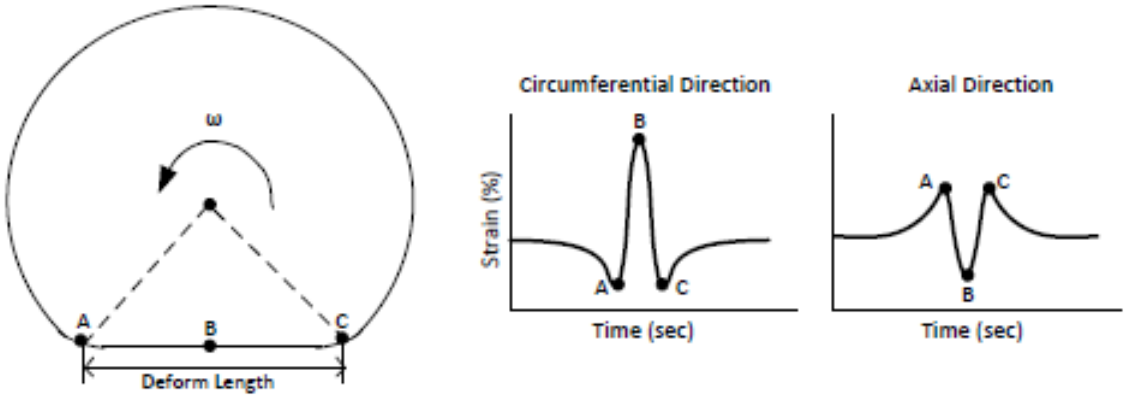

Figure 3: Symmetrical longitudinal and lateral strain gauge trends for straight-line driving from literature (adapted from Morinaga et al., 2006). Three key points in the contact patch are shown (left) and the circumferential (middle) and axial (right) strain distribution is shown along this length

Strain in the longitudinal and lateral direction are seen to be symmetrical at steady state conditions. The symmetrical shape is due to the tyre deforming from a circular shape to flat when in contact with a flat surface. A passenger car tyre is relatively smooth in comparison to an agricultural tyre. The strain on an agricultural tyre should, however, have an overall similar trend due to the same deflection from round to flat with compression and tension created in the contact patch. However, the lugs were seen by Feldesi et al. (2020) to have a significant effect during static test, with abrupt strain changes caused by the lug. While (Garcia-Pozuelo et al., 2017a, Garcia-Pozuelo et al., 2019 and Morinaga et al., 2006) presents results from point measurement along the centreline, one could apply more gauges to measure the strain of different circumferential paths. This would however require a more complex data acquisition system to handle multiple strain gauges and the resolution in the circumferential direction is limited by the strain gauge size.

From literature, the strain within the contact patch was determined to be dependent on several factors, one being the tyre structure. The circumferential locations of strain gauges also show no significant difference in the strain measurement on passenger car tyres due to the more uniform tread pattern. Strain distributions in an agricultural tyre are largely non-homogeneous with very abrupt changes in the proximity of the lugs, as shown by Feldesi et al. (2020) during static tests. Thus to ensure measurement sensitivity the results from static tests were used to find locations of high strain concentrations which would be suitable for the placement of strain gauges. The locations were not optimised to predict parameters such as slip angle or camber, as such results were not available, but rather areas of high strain sensitivity.

An inflation test of the agricultural tyre tested by Feldesi et al. (2020), as seen in Figure 4 with the longitudinal strain presented at the top and lateral strain at the bottom, aids in locating the lugs within the contact patch. The reference state is an unloaded fully deflated (0kPa) tyre. As the inflation pressure increases within the tyre's working pressure range, strain concentrations, in the longitudinal direction, appear around the location of tread blocks. It is noted that the strain distribution is non-homogenous, yet still has a repeating pattern.

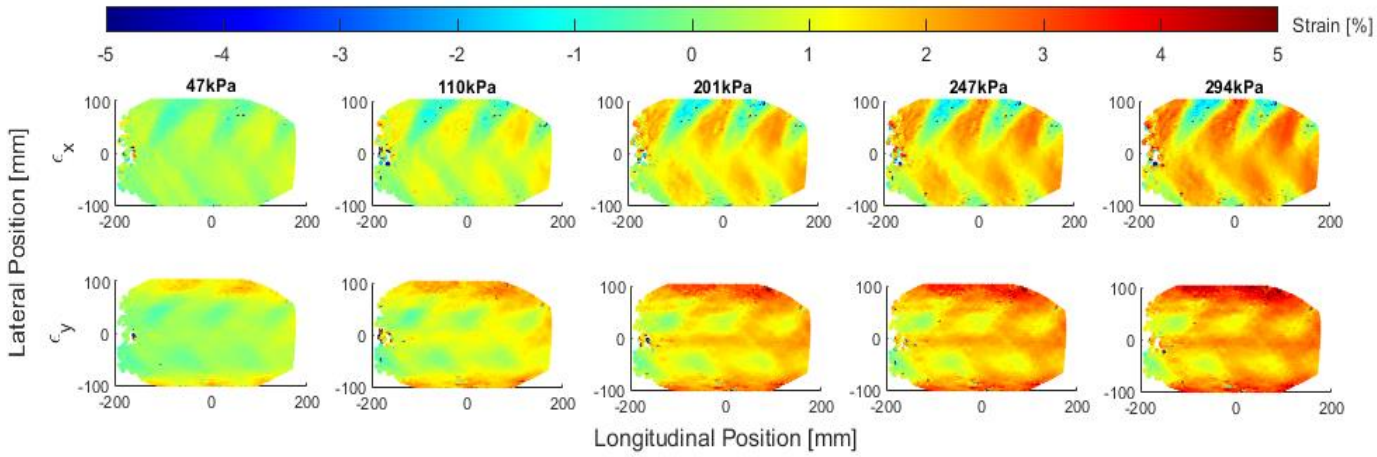

Figure 4: Discrete longitudinal and lateral strain with increase in inflation pressure

A vertical test at 200kPa is shown in Figure 5 where the unloaded tyre inflated to 200kPa is used as the reference state. The longitudinal (top) and lateral (bottom) strain can be seen at discrete instances with increasing vertical load. Peak longitudinal strains are seen to occur at the lateral edges of the contact patch, with strain values increasing

along the length of the lug with an increase in vertical load. Positions along the lengths of the lugs are thus a suitable location for strain gauge placement.

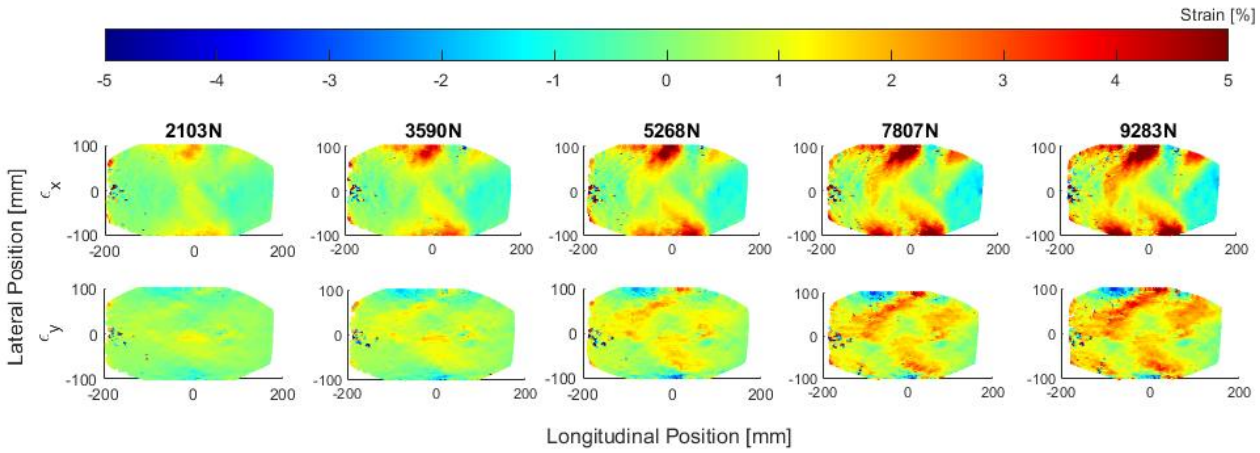

Figure 5: Discrete longitudinal and lateral strain with increase in vertical load at 200kPa

A single lug was chosen to place strain gauges along. Passenger car tyres tend to have ideal placement in the lateral centreline of the tyre, however in the case of the tested tyre locations along the lug showed higher strain sensitivity. Three point measurement locations were selected, based on the vertical and inflation test, are shown on the strain distributions of other loading conditions in Figure 6. The figure shows the strain distribution for a variety of tests including inflation, vertical load, longitudinal and lateral static tests.

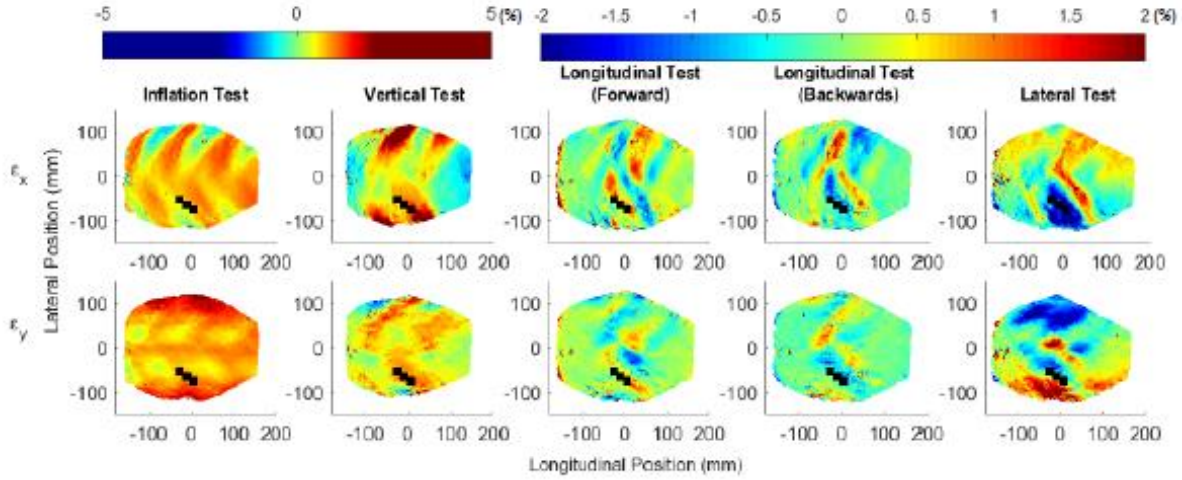

Figure 6: Inflation test, Vertical Test, Longitudinal Test (forward), Longitudinal Test (backward) and Lateral test on an agricultural tyre (200kPa)

The strain gauge placement was done from static test data which lacks phenomena only occurring in dynamic testing, therefore, the initial placement may be useful to understand the comparison of point to full-field measurements. Further refinement could be to optimise strain gauge placement with strain data from dynamic tests.

The strain range of static data does not exceed ±10% strain. The Micro-Measurements EP-08-125TM-350 strain gauges were used which has a strain range of ±20% and a temperature range of -75°C to 205°C. If tests are performed over short intervals the temperature limits will not be exceeded. The XY rosette strain gauges were selected such that configurations and directions could be easily changed, once installed.

Measurement of rubber is not a common application for strain gauges, even less so on a curved surface such as the inside of a tyre. Many Wheatstone bridge configurations cannot be used as many of them require symmetrical applications, with constant strain. The strain gauges will thus only be wired to a half or quarter bridge configuration. The half bridge requires knowledge of the Poisson's ratio which can be estimated by comparing lateral and longitudinal strain within the applied region. Temperature compensation was not considered as testing was kept to short intervals, however this would need to be considered in commercial applications. A free rolling test was done at the start of each test to obtain the initial strain prior to loading which is used to zero the strain gauges. The recommended adhesive was used, a Micro-Measurements M-Bond A-12 Adhesive, which could reach ±20% strain which is desirable to match the strain experienced by the gauges. Installation of the strain gauges included cleaning and smoothing the surface with sand paper. The gauges were applied to the test surface with the adhesive, a G-clamp was then used to keep the contact between the two and the tyre was then left to cure at room temperature for a period of two weeks.

2.4 Comparison Between Strain Gauge and Full Field Measurements

A very important aspect of agricultural tyres is the non-homogeneous tread pattern which was shown to create non-homogenous strain pattern during static tests. While the strain gauges are useful to provide a clearer picture of a single location on the tyre, other effects can be highlighted more clearly with a full-field strain measurement system. With a large lugged tyre, even when keeping all tyre operating conditions constant, the contact patch will constantly be changing due to the lug pattern. Thus, as the tyre rolls, the tyre contacts the road with different quantities of lugs and at different locations. This would result in continual variation of the strain produced in the contact patch. This makes it difficult to compare strain at different circumferential locations where the contact between the tyre and road differ due to the lugs, as the boundary conditions are not the same. Thus, only regions which exhibit the same contact boundary condition can be directly compared. Thus, full-field measurement which provide a strain pattern of the entire contact patch cannot directly be compared to the point strain measurements. This is due to the full-field measurements having a single boundary condition compared to the ever changing boundary condition of the point measurements.

Measurements from the full-field strain system were compared to the strain gauges by tracking a point from when it enters until it leaves the contact patch. This was done by placing a fictitious marker on the contact patch and following it through the contact patch in sequential images while it is in view by T2Cam. This ensures that the measurement should have the same boundary condition at every rotational angle.

2.5 Test Setup and Procedure

The experiments took place in an indoor tyre test rig, as shown in Figure 7, which can vary speed, vertical load and slip angle. The tyre was dynamically tested on a rolling drum of radius 0.8m. The test tyre is mounted on a hub fixed on a sliding mount which is used to vertically load and unload the tyre onto the drum. The vertical load applied to the tyre is measured by a Universal Low-Profile (ULP) load cell, which is installed between the sliding mount and where the force is applied. The wheel hub can be rotated to vary the tyre's slip angle to a range of -15° to 15°.

Figure 7: Dynamic test setup with test tyre installed

The test tyre was instrumented with the strain gauges and T2Cam. The camera system of T2Cam, can capture an image pair approximately every 2° per sample. The strain gauges are sampled at 1000Hz, which results in a measurement at least every 0.2° at the test speed of 5km/h. The strain gauges measurements were collected using an in house developed telemetry system which rotates with the tyre. The strain gauges on the inner surface were wired through an airtight gland to the outer telemetry. The layout of the strain gauges within the inner surface contact patch is shown in Figure 8. The tyre data acquisition system, which samples the strain gauges, is equipped with an absolute encoder that is used to synchronize the images captured by T2Cam. The synchronisation was achieved by a small dead region on T2Cam which always occurs at the same encoder reading. The encoder and strain gauges were sampled on the same data acquisition system and where therefore already synchronised. Synchronisation between strain gauges and T2Cam images were therefore possible by using the amount of images and time between images, with drift removed due to the dead band at every revolution of the tyre. It was seen during post-processing that the half bridge strain gauge began to debond during testing thus only the two quarter bridges' results were analysed.

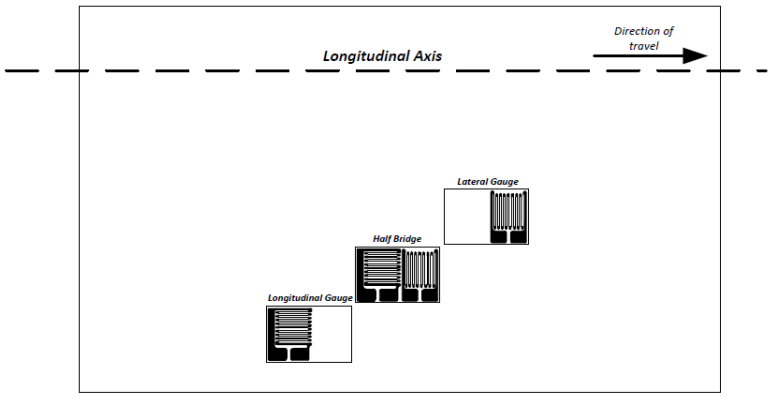

Figure 8: Layout and configurations of strain gauges placed within the inner surface contact patch

All tests were conducted at 5km/h. From literature it was determined that the strain measured inside a rolling tyre is affected by several conditions, with the following investigated in this study:

- Inflation pressure
- Vertical load
- Slip angle

The sensitivity to inflation pressure and vertical load was investigated by conducting initial tests at the following three different tyre pressures 120kPa, 160kPa and 200kPa. At each inflation pressure, two different vertical loads were applied, 700N and 1400N, while the tyre rotated freely on the drum at the test speed. A more comprehensive vertical load test was conducted by performing tests at different vertical loads from 50N to 2750N, at an inflation pressure of 200kPa. During the vertical and inflation tests the tyre was set to a slip angle 0°. All tests began with the tyre and drum initially stationary and the tyre not in contact with the drum. The drum would first be brought to a steady state speed before the tyre was incrementally loaded onto the drum. At each load increment the tyre was allowed to rotate at least one revolution before increasing the load. The reason for this procedure was due to the low motor torque which could not rotate the drum when initially loaded. The low motor torque also resulted in the drum speed slowly decreasing when the vertical load was increased. The load was increased until the drum could no longer handle additional load and the test was ended. No speed dependency tests were performed, and tests were all done at the same initial speed of 5km/h. The test procedure for the slip angle tests are very similar except that the tyre was set to a specific slip angle before loading onto the drum. The tyre was tested at five slip angles namely

3.22°, 2.15°, 1.16°, -1.67° and -2.68°. The width of the drum limited the testing to small slip angles as the higher slip angles resulted in the tyre not making proper contact with the drum and also affected the maximum vertical load which could be achieved due to the additional load on the motor.

3. Results and Discussion

3.1 Tyre Inflation Pressure Effect

Inflation pressure contributes to a stiffer tyre and therefore results in smaller tyre deformations. The effect of inflation pressure on the strain profile was tested on a rolling tyre. The strain distribution of the rolling tyre tested at two different vertical loads and three different inflation pressures is shown in Figure 9.

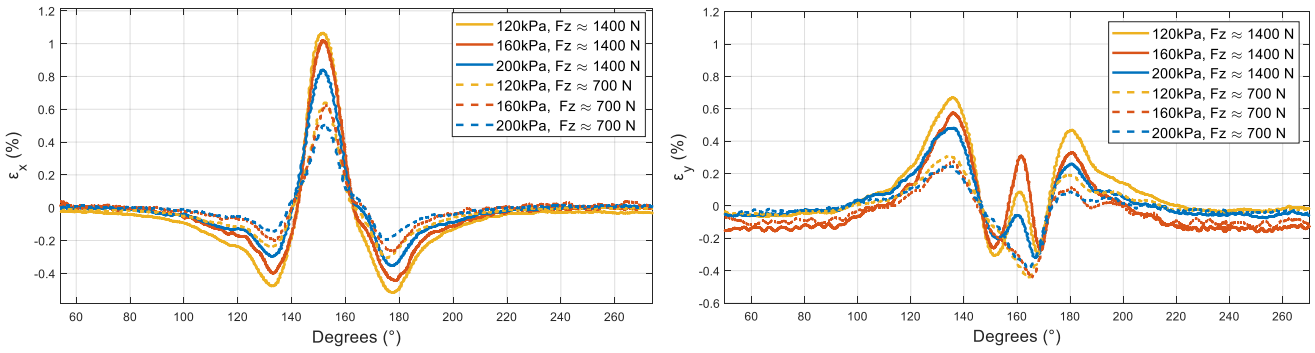

(a) (b)

Figure 9: (a) Longitudinal strain, (b) Lateral strain results at two vertical loads and inflation pressures of 120 kPa, 160 kPa and 200 kPa

It is evident that the longitudinal strain shows the same strain curve per revolution found on passenger car tyres, consisting of two compression peaks and one tension peak. It is also evident that the vertical force has a much larger effect on the strain peaks compared to the inflation pressure. The trend of the tension and compression peaks as a function of inflation pressure is as expected. Higher strain peaks are obtained at lower inflation pressure due to the tyre being less stiff. The circumferential location of peak strains does not appear to change with a change in inflation pressure but does change slightly due to a change in vertical load. Since the vertical load has a large influence on the strain profile and the tyre pressure is easy to measure using other means the effect of vertical load is studied more closely.

3.2 Vertical Load

The effect of vertical load on the strain profile is investigated at an inflation pressure of 200 kPa. The full longitudinal strain profile measured by the longitudinal strain gauge is shown in Figure 10. Similar to the trends seen by Morinaga et al. (2006), a tension peak occurs at the centre of the contact patch (≈150°) and two compression peaks as the gauge enters and leaves the contact patch (≈130° and 180°). Changes due to load can be noted by the increase in these tension and compression peaks, while the areas far removed from the contact patch remain unaffected. The same sensitivity to vertical load was seen by Garcia-Pozuelo et al. (2017a). The location of the maximum tension peak occurring at approximately 150° is seen to shift to the left with increase in vertical load as seen in the right plot of Figure 10.

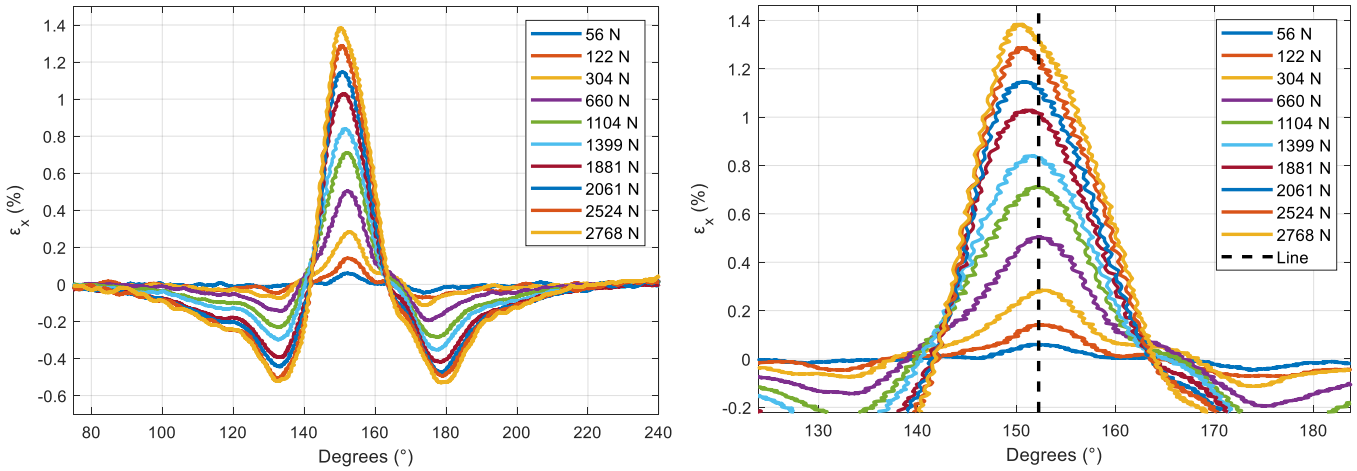

(a) (b)

Figure 10: (a) Longitudinal strain gauge results with increase in vertical load (200kPa, 5km/h) (b) zoomed in region longitudinal strain

The longitudinal strain profile experiences a tension strain at the centre of the contact patch, with the magnitude increasing at higher vertical loads. The centre of the contact patch for the lateral strain distribution, as shown in Figure 11, experiences larger fluctuations at higher vertical loads. At low vertical loads there is a prominent tension peak at approximately 150° and compression peak at approximately 165°. As the vertical load increases, an additional tension peak occurs at approximately 165° as the compression peak turns into a tension peak. This creates three tension peaks spaced roughly 21° degrees apart with the centre peak showing the largest sensitivity. The tension

peak spacing of 21° corresponds to the lug spacing as there are 17 lugs on each side of the tyre, which indicates that each of these peaks could be due to a lug in contact with the drum. The lower loads may only have a single lug in contact which could explain the increase in the number of tension peaks as the vertical load increases.

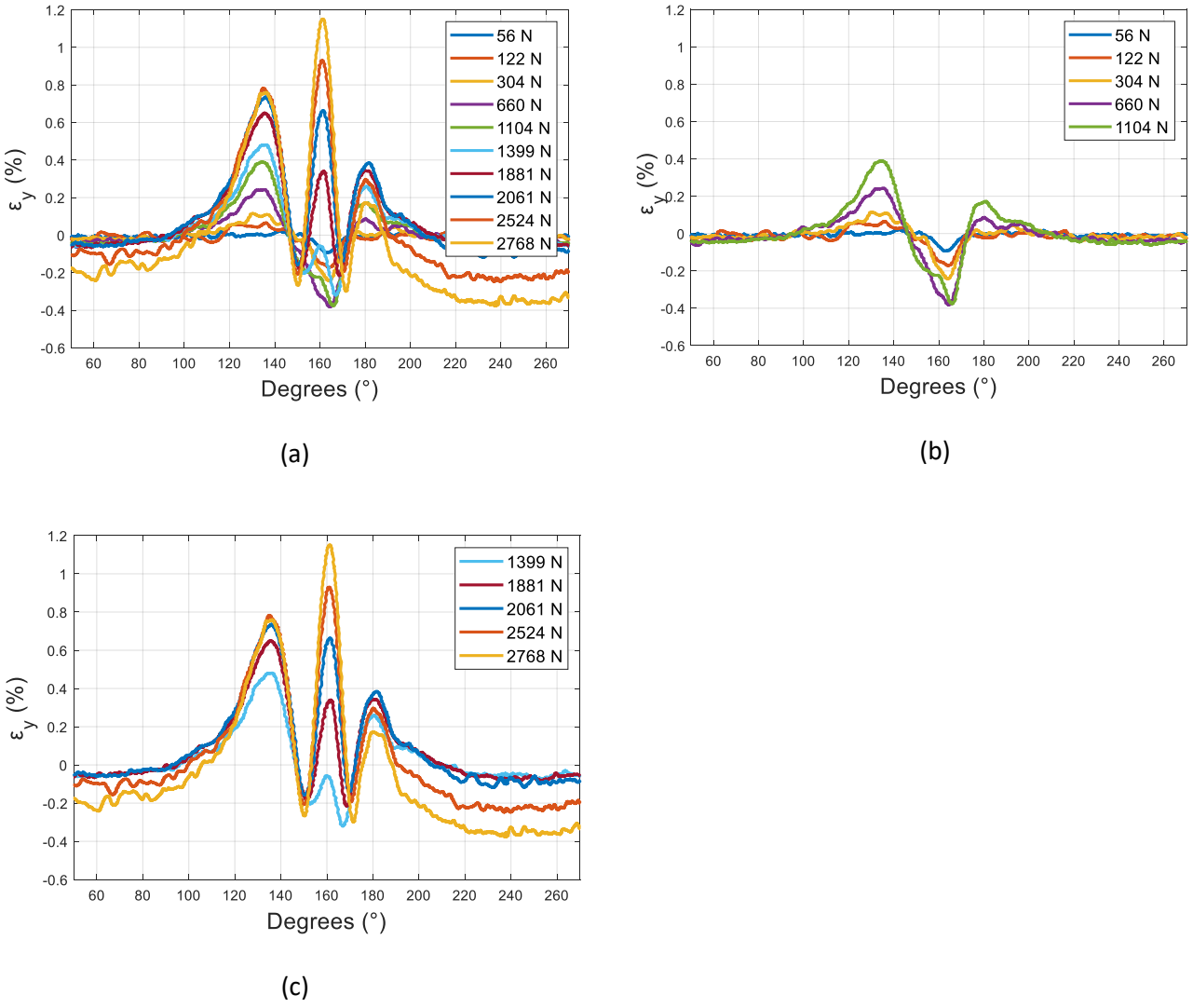

Figure 11: Lateral strain results with increase in vertical load at 200kPa. (a) all vertical loads and (b) low vertical loads up to 1100N (c) higher loads from 1400N to 2768N

Feldesi et al. (2020) obtained linear relationships between point strain locations and the loading conditions during static vertical tests. The strain of certain points on the strain profile, indicated in Figure 12, show the largest sensitivity to changing factors. These points will be used to fit linear relationships between the strain and the vertical load. The lateral strain showed a significant trend change at higher loads. Thus, the lateral strain is differentiated

between low load and high load in Figure 12B and Figure 12C respectively. The changes in lateral strain from Garcia-Pozuelo et al. (2017a) showed a reduction in the compressive peak magnitude but the compressive peak did not turn into a tension peak as was found in this study. The two compression peaks in Figure 12C were seen to be equivalent in most cases and therefore were not individually measured.

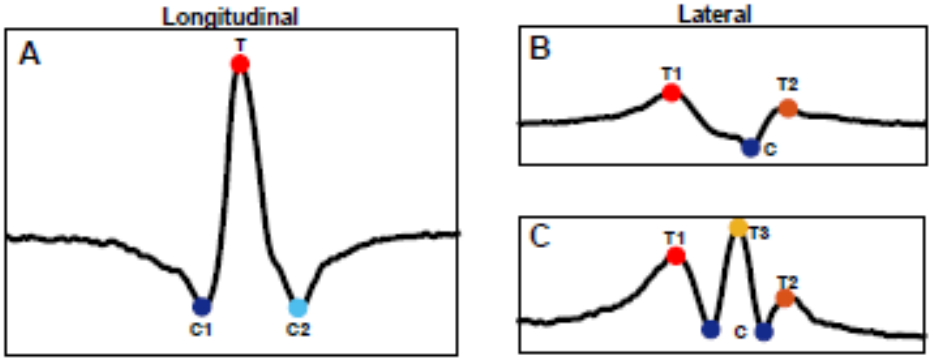

Figure 12: Key points for measurement for the inner surface strain distribution in the (A) longitudinal direction and the lateral direction at (B) low loads and (C) larger loads

The change in strain at the identified key points, shown in Figure 12, with an increase in vertical load is shown in Figure 13. The longitudinal strain has a linear relationship with vertical load for both tension and compression peaks (Figure 13(a)). The coefficient of determination (R^2) is above 0.97 for all the key points of measurement for the longitudinal strain. Most of the lateral strain key points experienced a less linear relationship to an increase in vertical load, with only T1 and T3 having a coefficient of determination (R^2) above 0.97. The lateral strain underwent a change in distribution at vertical loads higher than 1250N which introduced a third tension peak (T3), T3 had the most linear relationship with increase in vertical load. The load at which T3 appears is low in comparison to the loads expected during normal working conditions (Load Index is 9810N at 200 kPa) therefore the relationship between T3 and vertical load can be useful when measuring sensitivity to vertical load on lateral strain. This peak also shows the highest sensitivity to a change in vertical load.

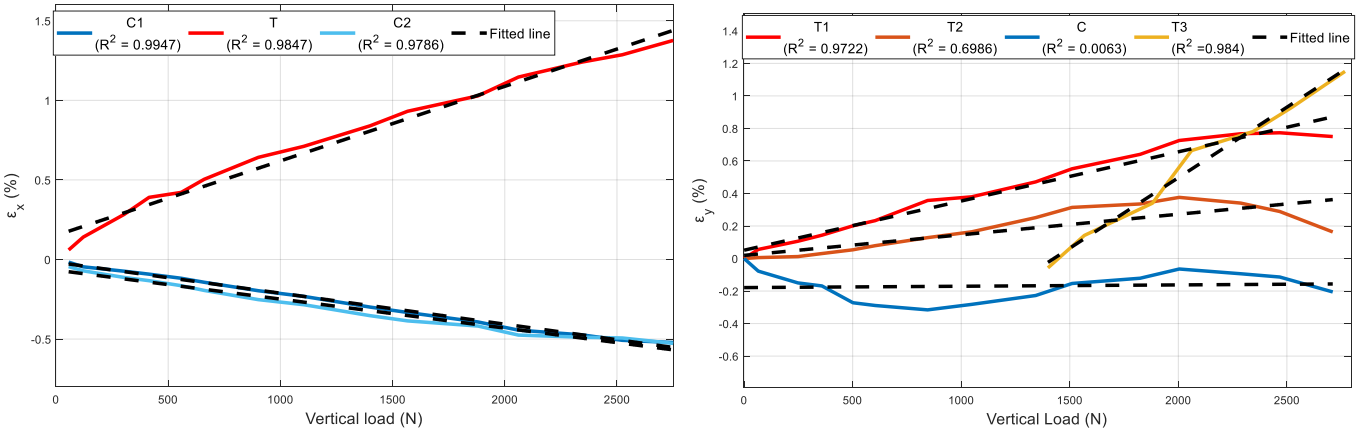

(a) (b)

Figure 13: Maximum (a) Longitudinal and (b) Lateral tension and compression peak strains during vertical loading at an inflation pressure of 200kPa

3.3 Slip Angle Tests

Each slip angle was tested at an initial speed of 5km/h and increasing vertical loads. The slip angle results at a vertical load of approximately 1600N is shown in Figure 14. The longitudinal strain, Figure 14 (a), shows very little change in the magnitude of the peaks. The most significant change is observed on the width of the profile. The width decreases at positive slip angles and increasing at negative slip angles. The lateral strain, Figure 14 (b), was shown to exhibit the highest sensitivity to a change in slip angle.

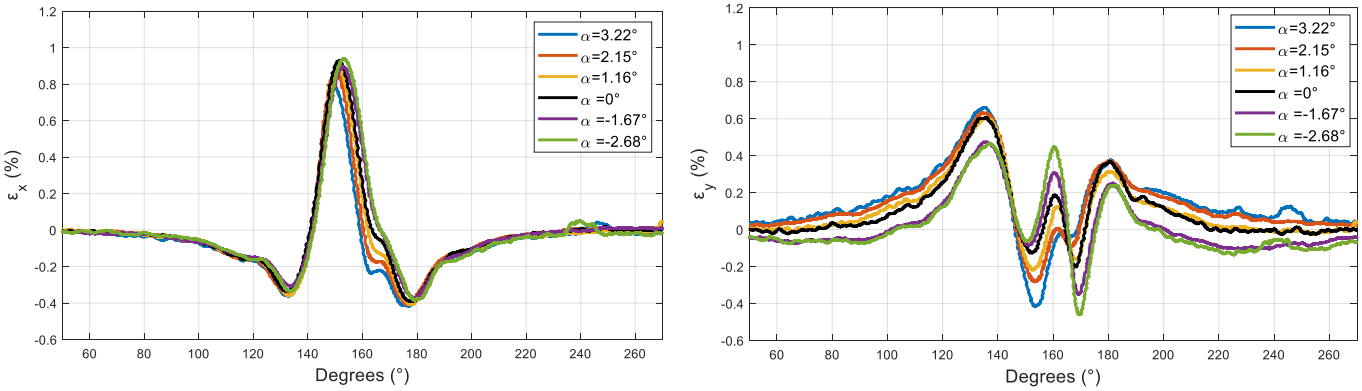

(a) (b)

Figure 14: (a) Longitudinal and (b) Lateral strain distribution for varied slip angles at a vertical load ≈1600N

The longitudinal and lateral strain peak values at different slip angles are shown in Figure 15. The T3 values are not shown for this plot as this peak was not always prominent at all slip angles as the vertical load was not high enough. The two compression peaks in the lateral strain distribution is the most sensitive to change in slip angle. The relationship is also very linear for the compressive peaks with coefficient of determination (R^2) above 0.92 for both and above 0.97 for C2.

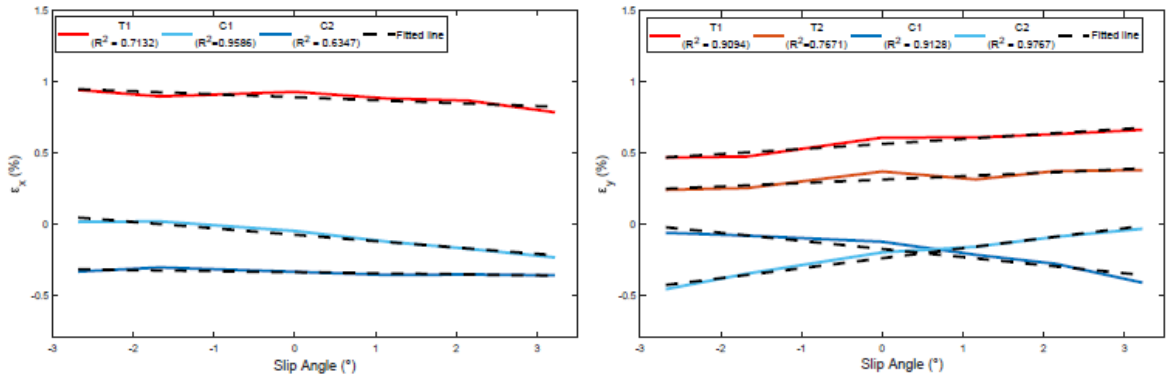

(a) (b)

Figure 15: Maximum (a) Longitudinal and (b) Lateral tension and compression peak strain measurements at different slip angles (≈1600N)

The results on agricultural tyres showed similarities with what is found in literature on passenger car tyres. However certain tests did have significant deviations which is postulated to be due to the lugs. Deviations in the strain distributions was seen in the lateral strain where the third tension peak was not commonly seen in literature, the three peaks were also spaced the same distance as the lugs apart. Useful linear relationships were still found between strain measurements and applied loads or slip angles which shows potential in using the measurement for tyre parameter and state estimation.

3.4 Comparison to Full Field Strain Results

The comparison at multiple vertical loads can be seen in Figure 16. The measurements could not be compared at the exact same location, due to the strain gauge lead wires obscuring the view of the inner surface. However, since the boundary conditions should be similar at 17 instances per revolution due to the repeating lug pattern, measurements could be compared on the sequential lug patterns.

Since the load cells are sampled at 1000Hz but the cameras are only triggered approximately every 2°, and at times trigger pulses were missed, comparison of points are relatively sparse. The longitudinal strain measurements correlate well and can be further improved with improvements to the camera sampling rate. However, the lateral results only show good correlation up to the second compression peak. The full-field measurements were seen to be very noisy towards the end of the contact patch which could affect correlation. The noise at the ends are attributed to the edge effects that occur with the algorithm as well as the edges appearing very small in one of the cameras which affects correlation. The reason for the worse correlation in the lateral strain compared to the longitudinal strain is unknown, it could be due to not using the exactly same location, this thus requires additional investigation. However, the technique has proven to be useful in evaluating the effect that lugs have on the strain distribution on the inside of the tyre due to the full field measurements. While the same could be done with multiple strain gauges this would require a more complex data acquisition system and has limited resolution capability due to the size of the strain gauges. Thus, the system can be used in further studies to further determine the effect that different lug patterns have on the strain distribution.

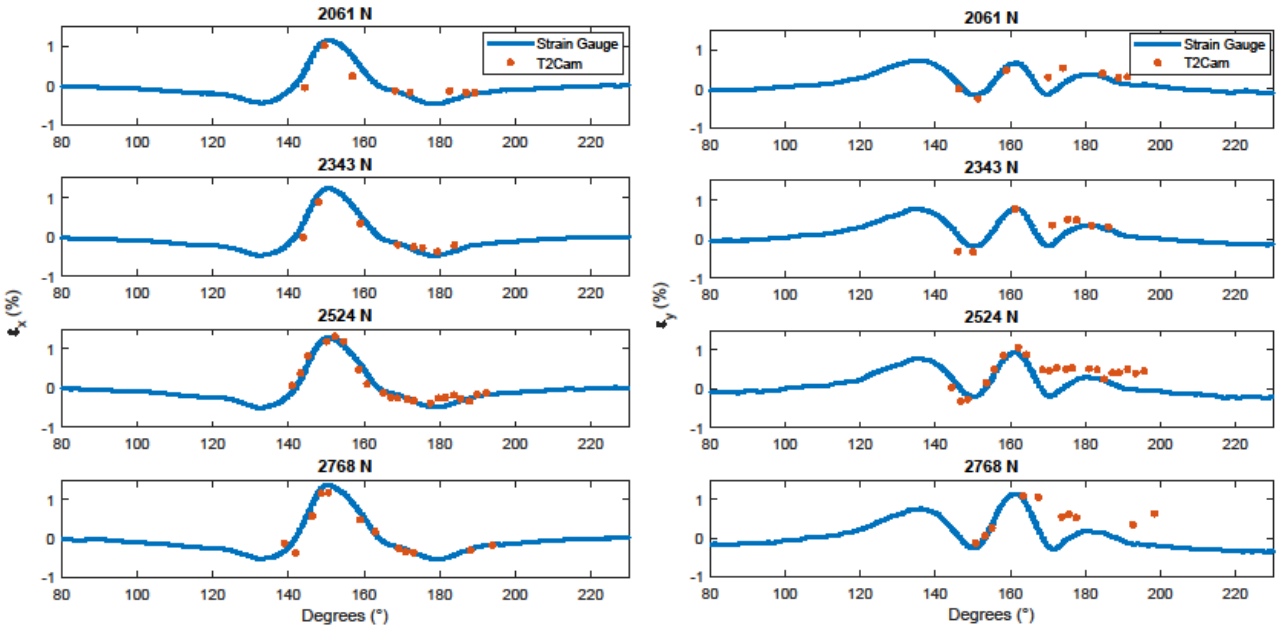

(a) (b)

Figure 16: Comparison of (a) Longitudinal and (b) Lateral strain from full-field and point measurements at three vertical loads (200 kPa, 5km/h)

The effect of the lug pattern in contact with the terrain is investigated using the full-field strain measurement system. Since there are 17 repeating lug patterns along the circumference of the tyre, it expected that the strain field is repeated approximately every 21°. Figure 17 shows the full-field longitudinal strain through one full cycle, 0-18.6°, at discrete angles. A tread pattern is overlaid to illustrate the movement of a tread pattern through the contact patch. The boundary conditions thus, due to the lug contact changing, does influence the produced longitudinal strain.

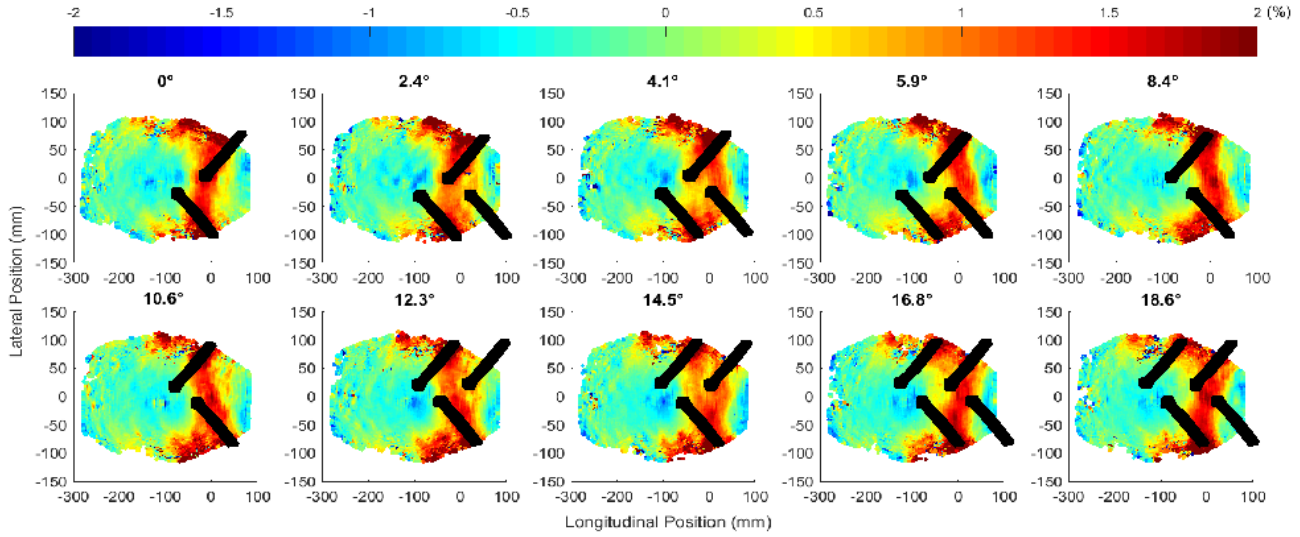

Figure 17: Longitudinal strain of discrete wheel rotation angles as tread block travels through contact patch

To better illustrate the mentioned effect, a waterfall plot of the longitudinal strain along a longitudinal section through the tyre at different rotation angles is created. The longitudinal section is taken at 20mm laterally and the waterfall plot is shown in Figure 18. The movement of the lugs through the contact patch can be visualised in this figure where the entry of a new lug can be seen with repeating patterns. Different angular regions experience different sensitivities and thus different magnitudes will be experienced at different circumferential measurement locations. This highlights the importance of circumferential point measurement location especially in an agricultural tyre. This needs to be considered when creating a standard measurement method for a tyre as it may require, if the location is not controlled for, that a calibration process be performed for each tyre to compensate for the differences

in location of the strain gauges. In passenger car tyre this may not be needed as the circumferential location has no effect.

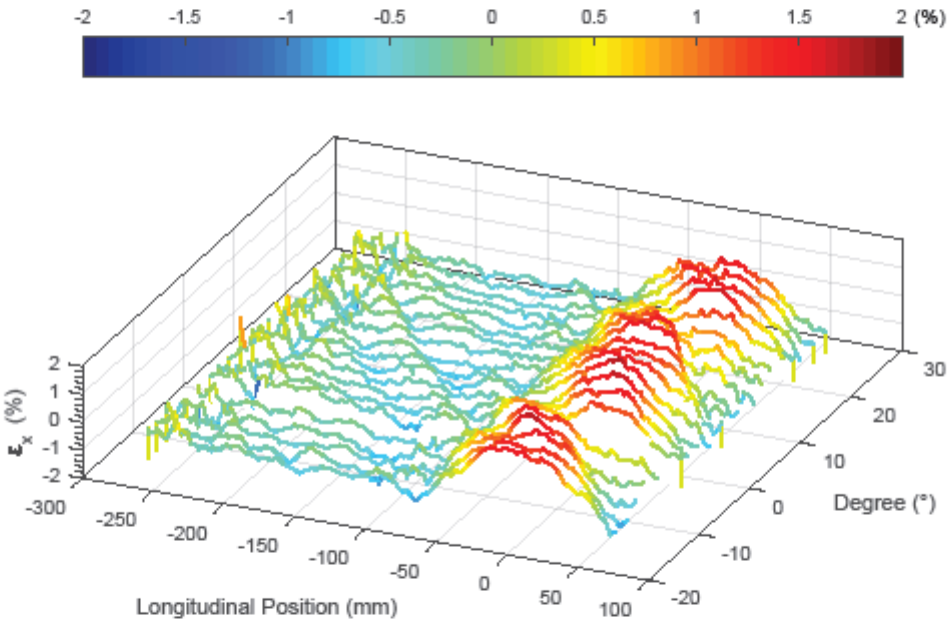

Figure 18: Waterfall plot of longitudinal strain showing movement of tread block through contact patch

4. Conclusion

Strain measurement, above acceleration and deflection, has shown to give insightful information of the contact patch and, when analysed, could lead to estimations of tyre states from strain measurements. The agricultural tyre is a complex tyre structure to predict tyre states as compared to passenger car tyres. The large lugs of the tyre were seen to influence the rolling tyre where noticeable differences were seen between the agricultural tyre and a passenger car tyre. The main trend of the strain profile is created when the tyre deforms its rounded surface when driven over a flat surface. Therefore, the main trend of the strain profile between passenger and agricultural tyres are comparable. Strain of passenger car tyres typically did not experience a prominent third tension peak in the lateral strain distribution, this effect is seen to be due to the large lugs contacting the test surface as the vertical load was increased and also showed high sensitivity to load changes. The tyre strain is dependent on many conditions and sensitivity to loading and boundary conditions were seen in full-field and point strain measurement. The longitudinal strain can be used for vertical force estimation, however, the longitudinal strain was insensitive to

changes in slip angle. The compression peak values for the lateral strain will be useful for lateral force estimation. The linear relationships seen between strain measurement and tyre loading conditions gives potential for a tyre which can be used to estimate tyre-terrain forces. Having this vital understanding of the tyre-terrain interface can lead to estimation of tyre states and parameters which can be used to enhance current safety systems. The use of both point and full-field strain measurement showed great potential and validates that strain can be used to measure important tyre parameters in a rolling tyre. Additional research can be performed using point and full field measurements to investigate the effect of different lug patterns.

5. References

Acosta, M., Kanarachos, S. and Fitzpatrick, M.E., 2017, July. A Virtual Sensor for Integral Tire Force Estimation using Tire Model-less Approaches and Adaptive Unscented Kalman Filter. In ICINCO (1) (pp. 386-397).

Armstrong, E.G., Sandu, C., and Taheri, S. - "Investigation into Use of Piezoelectric Sensors in a Wheeled Robot Tire for Surface Characterization", J. of Terramechanics, Special Issue on Robotic Vehicles, Vol. 62, pp. 75-90 (16), doi:10.1016/j.jterra.2015.07.003, 2015.

Maurya, P. K. et. al. - "Energy harvesting and strain sensing in smart tire for next generation autonomous vehicles", Applied Energy, Vol. 232, pp. 312-322, doi.org/10.1016/j.apenergy.2018.09.183, 2018.

Baker S and Matthews I. 2004. Lucas-Kanade 20 years on: a unifying framework. Int J Computational Vision 56:221–255

Botha, T. R., Guthrie, A. G., Jiminez, E., Els, P. S. and Sandu, C., 2017, Tyre Longitudinal Velocity and Slip Measurements from the Inside of a Tyre. 19th International & 14th European-African Regional Conference of the ISTVS, 25.-27.09.2017 Budapest. In: Proceedings of the 19th International & 14th European-African Regional Conference of the ISTVS, S.1–10

Botha, T. and Els, S. (2014). Rough Terrain Vehicle Side-slip angle measurement using digital image correlation. Proceedings of the 18th International Conference of the ISTVS.

Braghin, F., Brusarosco, M., Cheli, F., Cigada, A., Manzoni, S., and Mancosu, F. (2006). Measurement of contact forces and patch features by means of accelerometers fixed inside the tire to improve future car active control. Vehicle System Dynamics, vol. 44 (sup1): pg.3-13.

Cao, S., Pyatt, S., Anthony, C., Kubba, A., Kubba, A., and Olatunbosun, O. (2016). Flexible Bond Wire Capacitive Strain Sensor for Vehicle Tyres. Sensors, 16(929).

Feldesi, F., Botha, T. R., and Els, P. S. (2020). Full-field strain measurements of the inside of an agricultural tyre using digital image correlation. Journal of Terramechanics, 91:309–318.

Garcia-Pozuelo, D., Olatunbosun, O., Strano, S., and Terzo, M. (2019). A real-time physical model for strain-based intelligent tires. Sensors and Actuators A, 288:1-9.

Garcia-Pozuelo, D., Olatunbosun, O., Yunta, J., and Yang, X. (2017a). A Novel Strain-Based Method to Estimate Tire Conditions Using Fuzzy Logic for Intelligent Tires. Sensors, 17(350):1-16.

Garcia-Pozuelo, D., Yunta, J., Olatunbosun, O., Yang, X., and Diaz, V. (2017b). A Strain-Based Method to Estimate Slip Angle and Tire Working Conditions for Intelligent Tires Using Fuzzy Logic. Sensors, 17(874).

Green, R. W. (2011). A Non-contact Method for Sensing Tire Contact Patch Deformation Using a Monocular Vision System and Speckled Image Tracking. Auburn University.

Guthrie, A.G., Botha, T.R., Jimenez, E., Els, P.S. and Sandu, C., 2017. Dynamic 3D measurement of tyre-terrain interaction. In 19th International and 14th European-African Regional Conference of the ISTVS. Budapest.

Guthrie, A. G., Botha, T. R., and Els, P. S. (2017). ScienceDirect 3D contact patch measurement inside rolling tyres. Journal of Terramechanics, 69:13-21.

Hamersma, H.A., Botha, T.R. and Els, P.S., 2016. The dynamic rolling radius of a pneumatic tyre on hard terrains. International Journal of Vehicle Systems Modelling and Testing, 11(3), pp.234-251.

Hiraoka, N., Matsuzaki, R., and Todoroki, A. (2009). Concurrent Monitoring of In-plane Strain and Out-of-plane Displacement of Tire Using Digital Image Correlation Method. Journal of Solid Mechanics and Materials Engineering, 3(11):1351-1357.

Khaleghian, S., Emami, A. and Taheri, S., 2017. A technical survey on tire-road friction estimation. Friction, 5(2), pp.123-146.

Lee, J., Oh, J., Kim, H., and Choi, B. (2015). Strain-based piezoelectric energy harvesting for wireless sensor systems in a tire. Journal of Intelligent Material Systems and Structures, 26(11):1404-1416.

Matilainen, M. and Tuononen, A. (2015). Tyre contact length on dry and wet road surfaces measured by three-axial accelerometer. Mechanical Systems and Signal Processing, 52-53:548-558.

Matsuzaki, R. and Todoroki, A. (2007). Wireless flexible capacitive sensor based on ultra-flexible epoxy resin for strain measurement of automobile tires. Sensors and Actuators A, 140:32-42.

Matsuzaki, R., Todoroki, A., and Kobayashi, H. (2005). Passive wireless strain monitoring of a tire using capacitance and electromagnetic induction change. Advanced Composite Materials, 14(2):147-164.

Morinaga, H., Wakao, Y., Hanatsuka, Y., and Kobayakawa, A. (2006). The possibility of intelligent tire (technology of contact area information sensing). FISITA World Automotive Congress, pages 1-11.

Niskanen, A. J. and Tuononen, A. J. (2014). Three 3-axis accelerometers fixed inside the tyre for studying contact patch deformations in wet conditions. Vehicle System Dynamics, 52(sup1):287-298.

Pohl, A., Steindl, R., and Reindl, L. (1999). The “Intelligent Tire“ Utilizing Passive SAW Sensors – Measurement of Tire Friction. IEEE Transactions on Instrumentation and Measurement, 48(6):1041-1046.